Pion production in $dp \rightarrow dN\pi$ reactions with deuteron projectiles

J. Greiff,[1,*,†] I. Koch,[1,*] W. Scobel,[1] H. Rohdjeß,[2] J. Dyring,[3] K. Fransson,[3] L. Gustafsson,[3] S. Häggström,[3] B. Höistad,[3] J. Johanson,[3] A. Johansson,[3] T. Johansson,[3] A. Khoukaz,[3] S. Kullander,[3] R. J. M. Y. Ruber,[3] J. Złomańczuk,[3] V. Dunin,[4] B. Morosov,[4] A. Sukhanov,[4] A. Zernov,[4] A. Kupść,[5] P. Marciniewski,[5] J. Stepaniak,[5] R. Bilger,[6] W. Brodowski,[6] H. Clement,[6] G. J. Wagner,[6] H. Calén,[7] C. Ekström,[7] J. Zabierowski,[8] B. Shwartz,[9] A. Sukhanov,[9] W. Oelert,[10] T. Sefzick,[10] and A. Turowiecki[11]

[1]*I. Institut für Experimentalphysik, Universität Hamburg, D-22761 Hamburg, Germany*
[2]*Institut für Strahlen– und Kernphysik, Universität Bonn, D-53115 Bonn, Germany*
[3]*Department of Radiation Sciences, Uppsala University, S-75121 Uppsala, Sweden*
[4]*Joint Institute for Nuclear Research, Dubna, RU-101000 Moscow, Russia*
[5]*Institute for Nuclear Studies, PL-00681 Warsaw, Poland*
[6]*Physikalisches Institut, Universität Tübingen, D-72076 Tübingen, Germany*
[7]*The Svedberg Laboratory, S-75121 Uppsala, Sweden*
[8]*Institute for Nuclear Studies, PL-90137 Lódź, Poland*
[9]*Budker Institute of Nuclear Physics, Novosibirsk RU-630090, Russia*
[10]*IKP, Forschungszentrum Jülich GmbH, D-52425 Jülich, Germany*
[11]*Institute of Experimental Physics, Warsaw University, PL-0061 Warsaw, Poland*

(Received 16 June 2000; published 13 November 2000)

Kinematically complete events have been studied for the reactions $dp \rightarrow dp\pi^0$ and $dp \rightarrow dn\pi^+$ at projectile energies between 437 and 559 MeV. The measurement covers a range of pion momenta $\eta = p^{\mathrm{max}}_{\pi,\mathrm{c.m.}}/m_\pi c$ from near the production threshold ($\eta = 0.32$) to $\eta = 0.86$ close to the $NN \rightarrow NN\pi$ threshold. The measurements were performed at the CELSIUS storage ring with the PROMICE/WASA setup. Angular and spectral distributions of the charged ejectiles as well as total cross sections are decomposed into the fractions that can be attributed to a quasifree $NN \rightarrow d\pi$ process with a spectator nucleon, and to a process involving all three nucleons. The quasifree contribution increases with energy and dominates from the $NN \rightarrow NN\pi$ threshold on. The results are compared to calculations with a spectator model with and without dp final state interactions.

PACS number(s): 13.75.Cs, 21.45.+v, 25.10.+s, 25.40.Qa

I. INTRODUCTION

Pion production in nucleon-nucleus collisions can be approximated as a production in the nucleon-nucleon ($2N$) system if the momentum distribution of nucleons in the nuclear environment is adequately taken care of [1–4]. Beyond that, three-nucleon ($3N$) forces may contribute [5–7], but they are expected to be small. In addition initial and final state interactions (FSIs) may come into play and obscure the elementary pion production process to some extent [8–10].

The $3N$ system given by the pd interaction is the easiest and most tractable one to investigate in this context. This is particularly true, if one wants to study the quasifree $NN \rightarrow NN\pi$ process, since the deuteron is loosely bound and the average distance between its two nucleons accordingly large. This work deals with a study of the reactions $pd \rightarrow pd\pi^0$ and $pd \rightarrow nd\pi^+$ between the $3N$ and the $2N$ pion production thresholds with focus on the quasifree (QF) contribution.

Above the $2N$ threshold, i.e., at proton projectile energies in excess of 280 MeV, the pion production in the pd system does not require the participation of a third nucleon for momentum conservation and it may act as a true spectator to the QF $NN \rightarrow NN\pi$ process. Its participation is needed below this energy, at least to the extent that its internal motion relative to the reacting nucleon provides the missing momentum for subthreshold pion production. This momentum, κ, becomes the higher as the $3N$ threshold at about 210 MeV projectile energy is approached, where it reaches 200 MeV/c. The probability density of the nucleon momentum in the deuteron peaks at $\kappa = 0$; the probability for having $\kappa = 200$ MeV/c is about a factor of 10^3 lower. In the QF reaction picture this converts into a corresponding drop of the production cross sections from μb to nb scales. This is a main reason why only a few studies of the $pd \rightarrow Nd\pi$ process have been performed up to 1990, only for energies far above threshold [11–14] and with limited statistics.

However, the advent of proton storage rings with cooled beams about ten years ago brought the study of the NN interaction in few nucleon systems to unprecedented levels of precision. The first—and so far only—study of the reaction $pd \rightarrow pd\pi^0$ between the $2N$ and $3N$ threshold was performed at the Indiana Cooler using an internal D_2 gas jet target and a forward detector for charged particles [15]. The excitation functions of the total cross section were interpreted in terms of a QF mechanism with $pn \rightarrow d\pi^0$ being the only contributing $2N$ channel [8]. The model gave the correct order of magnitude (within a factor of 5) for the cross section and the steep drop when approaching the $3N$ threshold could be attributed to the target deuteron wave function. The correct energy dependence, however, could only be reproduced with the inclusion of a pd-FSI of Watson-Migdal

*Present address: Department of Radiation Sciences, Uppsala University, Uppsala, Sweden.
†Corresponding author.

type [16] and an overall normalization. The authors [8] then conclude from the excitation function, that the main properties of the $pd \to pd\pi^0$ reaction near threshold can be explained by this QF model.

The most straightforward way to verify this experimentally is to investigate the angular and energy distributions of the supposed spectator proton, which should reflect the initial momentum distribution in the deuteron. This analysis of the $pd \to pd\pi^0$ data together with supplementary data acquired concurrently for the isospin related channel $pd \to nd\pi^+$, yielded results which were incompatible with a dominance of the QF mechanism [17]. The differential cross sections close to the $3N$ threshold ($\eta \leq 0.5$) rather point towards a more uniform phase space population. The QF mechanism starts to be important close to the $2N$ threshold and is concentrated in regions of the phase space where the target nucleons have low momenta in the laboratory frame. This condition, however, excludes direct nucleon spectator spectroscopy. It was indirectly accessible in the $pd \to nd\pi^+$ reaction via detection of the d but it was limited by the detector acceptance for the π^+.

These restrictions can be overcome by increasing the acceptance with a detector of larger solid angle coverage, and some capability for π^0 and π^+ detection, and by using *deuteron projectiles* in conjunction with an internal *hydrogen target* to boost the energy of the spectator nucleons. The study presented here includes improvements along these lines to quantify the quasifree mechanism in the $dp \to dN\pi$ reaction between the $3N$ and the $2N$ threshold. Here, $2N$ threshold means the minimum projectile energy needed for pion production, where one of the two projectile nucleons interacts with the target proton, whereas the second continues as spectator with the initial beam velocity. The paper is organized as follows. Section II gives a description of the detector and the measurements. In Sec. III we discuss possible reaction mechanisms, models, and the Monte Carlo simulations. Section IV contains details of the data analysis followed by the experimental results on $dp \to dp\pi^0$ and $dp \to dn\pi^+$ and their comparison to model calculations. Our conclusions are summarized in Sec. V.

II. EXPERIMENTAL SETUP AND MEASUREMENTS

A. General

The experiment was performed at the Cooler Synchrotron CELSIUS of the The Svedberg Laboratory with a deuteron beam impinging on an internal hydrogen cluster jet target. Measurements were carried out at five different projectile energies between the $dp \to dp\pi^0$ and the $pn \to pn\pi^0$ threshold. They are listed in Table I, where the energy in excess of the pion production threshold is expressed as $\eta = p^{\max}_{\pi,\mathrm{c.m.}}/\mathrm{m}_\pi c$ with $p^{\max}_{\pi,\mathrm{c.m.}}$ being the largest center-of-mass pion momentum in dimensionless units. The thresholds for QF pion production in the $2N$ subsystem $pn \to d\pi^0$ ($pp \to d\pi^+$) at $\eta = 0.83$ (0.84) are slightly above (below) our highest deuteron projectile energy. The two production runs were separated by half a year and the lowest projectile energy was repeated in the second run for a consistency check.

The CELSIUS storage ring [2] was filled with typically 2×10^9 deuterons; their stripping injection and subsequent acceleration took about 30 s. The coasting beam was then used for up to 540 s without noticeable intensity loss. Electron cooling was applied at the two lowest energies $T_d = 437$ and 454 MeV to improve the signal-to-background ratio for these runs. At the end of this *flattop* interval the beam was dumped and within 30 s the next cycle started.

B. Target and PROMICE/WASA detector

The experiment used the PROMICE/WASA setup and is shown schematically in Fig. 1. It can be divided into the target system, the central detector (CD) for photon and charged particle detection, and the forward detector (FD) section for charged particles.

The target [18] was operated with pressurized H_2 gas that is vertically injected through a nozzle cooled to 20–30 K into the interaction region. At the intersection with the CELSIUS beam the jet forms a beam of 6.5 mm diameter across and 10.5 mm along the direction of the circulating projectiles. The typical areal thickness was 1.3×10^{14} cm^{-2} which resulted in typical luminosities of $1-2 \times 10^{29}$ cm^{-2} s^{-1}.

The central detector consists of two 7×8 arrays of CsI(Na) modules on each side of the beam. They constitute electromagnetic calorimeters (CEC) with thickness of about 16 radiation lengths and cover an angular range of $\pm 30° \leq \Theta_{\mathrm{lab}} \leq \pm 90°$ and $-25° \leq \Phi \leq +25°$ with respect to the horizontal plane. Thin scintillator bars (CFB) in front of the CECs allow to veto charged particles. In addition there are upstream counters to veto beam halo events.

The forward detector covers angles Θ_{lab} from 4° to 22° with a sequence of detectors to provide particle identification and momentum by direction and pulse height measurements. A segmented thin (3 mm plastic scintillator) window counter (FWC) serving as trigger on charged hadrons is followed by two sets of proportional drift chambers (FPC) to determine x and y coordinates for tracking, and by a combination of a scintillator hodoscope (FHD) and range hodoscope (FRH).

The FHD consists of 5mm thick scintillators, one layer of 48 radial shaped elements, preceded by two layers with 24 elements, bent as Archimedian spirals with opposite helicity. They comprise 1104 triangular pixels [19] for particle identification via ΔE, hit multiplicity measurement, and track separation. The four layers of the FRH, each being 11 cm thick, are sufficient to stop deuterons (protons, charged pions) with kinetic energies up to 400 MeV (300, 170 MeV). The downstream veto (FVH) finally allows to separate stopped from penetrating charged particles. A more detailed description of the detector is given in Ref. [20].

C. Luminosity measurement

The absolute luminosity was obtained from a concurrent measurement of elastic dp scattering at small ($5° \leq \Theta_{\mathrm{lab}} \leq 15°$) scattering angles. The forward going deuteron was identified in the FD, and the recoiling proton was detected with silicon strip detectors with nine vertically oriented strips of 300 μm thickness and 5 mm$\times$20 mm area. They were placed outside of the scattering chamber behind the thin (0.5

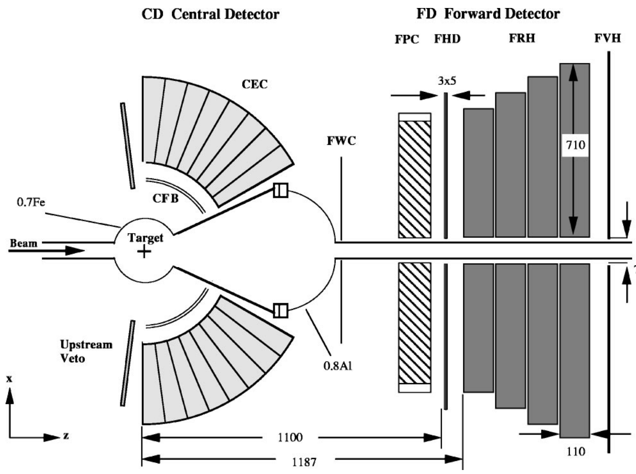

FIG. 1. The PROMICE/WASA detector at the CELSIUS storage ring.

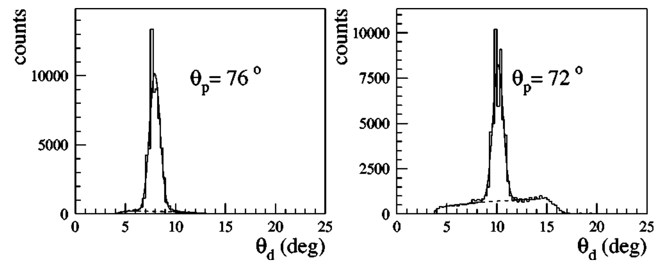

FIG. 2. Deuteron angular distributions for $T_d = 455$ MeV in coincidence with recoiling protons in detector strips at $\Theta_p = 76°(72°) \pm 0.65°$. The dashed line indicates the background subtraction.

mm stainless steel) window. A minimum proton energy of 12–15 MeV was required for unambiguous proton detection. Elastic scattering events were identified from (i) the coplanarity and (ii) a kinematically correct opening angle Θ_{dp}. The latter also allowed for separating these events from background events of the breakup reaction $dp \rightarrow npp$, see Fig. 2.

The systematic error associated with the luminosity measurement results from the uncertainty of the reference data [21] for elastic pd scattering (8%), and from the scatter of the angular distribution measured with the strips as compared to the reference value, which amounted to 5% (15%) for the second (first) run period.

D. Triggers

The total event rate in the WASA/PROMICE setup was in the order of 10^5 Hz. A two level hardware trigger brought this to an event rate less than 1 kHz. The main physics trigger (referred to as TI) required two coincident hits in the window counters (FWC), the first two layers of the forward hodoscope (FHD), and no hit in the downstream veto (FVH), to select events with two charged particles stopped in the FRH. The veto condition helped to suppress breakup events $dp \rightarrow npp$ with energetic protons, without affecting the pion producing channels. Trigger TI was combined in offline analysis with the request of at least one neutral (i.e., no signal in the CFB) hit in one of the two CsI arrays comprising the CD. This combination is referred to as trigger TII in the following.

Additional triggers were set up for coincidences of neutral hits in the two parts of the CD for offline identification of the π^0 decay, for LED generated light pulser events [22] to monitor the gain of the detectors, for the luminosity measurement via elastic dp scattering, and for subevents controlling the FHD, the FRH, the CEC, and the CFB veto detectors offline. These triggers were prescaled for proper adjustment of the trigger rates.

E. Detector calibration and particle identification

The particle identification makes use of the trigger mode, in combination with hit pattern and pulse height information obtained from the components of the detector subgroups. All elements of the FRH and the third layer of the FHD were read out via long-range multihit TDCs, in addition, to record delayed pulses. This information supplemented the π^+ identification.

The position dependent energy calibration of the FD plastic scintillators was obtained with dedicated pp elastic scattering runs at $T_p = 400$ MeV. The light response to deuterons and π^+ was explored using the exit channel $pp \rightarrow d\pi^+$ based on this calibration. Following [23], the results were parametrized in light response functions $L(T) = a_1 T - a_2(1 - \exp a_3 T^{a_4})$ of the kinetic energy T of a stopped particle (p, d, π^+) with fit parameters a_i.

The CsI crystals were calibrated with photons from the $\pi^0 \rightarrow 2\gamma$ decay, where π^0's of known energy were produced in $pp \rightarrow pp\pi^0$ reactions with identification of the two charged particles in the FD. As a result, the reconstructed invariant mass $m_{\gamma\gamma}$ showed a width of about 10 MeV (σ).

The identification of charged particles p, d, π^+ is based on the energy loss of penetrating and deposited energies of stopped particles. The discrimination of deuterons against the more copious protons is most crucial for our experiment. Software cuts were carefully explored by first determining the loci of protons from supplementary measurements of, e.g., $pp \rightarrow pp\pi^0$ and $pp \rightarrow d\pi^+$ events. Deuterons were then identified in $dp \rightarrow dp\pi^0$ reactions with trigger TII and reconstruction of the missing pion mass. The upper part of Fig. 3 shows that, whenever necessary, the cuts were set close to the deuterons to minimize misinterpretation of protons. This way a small fraction of events with deuterons in the exit channel may be lost due to the finite energy resolution and the impact of dead detector material.

Deuterons will undergo nuclear interactions with the scintillator material and, in particular, break up with a nonnegligible probability in the FRH. This effect was investigated with the $pp \rightarrow d\pi^+$ events taken at $T_p = 400$ MeV. The bottom part of Fig. 3 shows that particles in correct angular correlation with the π^+ are identified as deuterons by their energy loss in the FHD, but some fraction deposits too little energy in the FRH and fails to be accepted as deuteron. The selection of deuterons in a small angular bin $\Theta_{\mathrm{lab}} = 7° \pm 0.5°$ yields not only the peak at $T_d = 170$ MeV, but also a low-energy tail. Monte Carlo simulations (see Sec. III D) reveal that only a small fraction in the tail is due to the competing $pp \rightarrow pn\pi^+$ channel; deuteron breakup in secondary

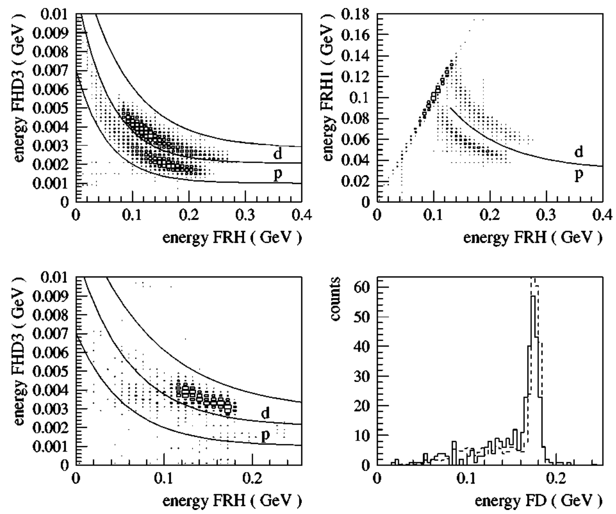

FIG. 3. The upper figures show the cuts used for particle identification in $dp \to dp\pi^0$ at $T_d = 559$ MeV. The lower left figure shows the same for $pp \to d\pi^+$ at $T_p = 400$ MeV and the lower right figure is the distribution of energy deposited in the FD by the subsample of particles emitted at $6.5° \leq \Theta_{\mathrm{lab}} \leq 7.5°$; the dashed line is the Monte Carlo simulation including d breakup.

reactions accounts for the major part. Additional examinations at different deuteron energies confirm that the energy dependence of these losses is well described by the simulations.

The π^+ identification was tuned with $pp \to d\pi^+$ events obtained in the calibration run with the TI trigger. In addition to the ΔE vs E signature, the π^+ candidates were requested to be followed by a delayed pulse from the $\pi^+ \to \mu^+ \nu_\mu \to e^+ \nu_e \nu_\mu \overline{\nu_\mu}$ decay ($\tau = 2.2$ μs) within 6 μs, either in the stopping FRH element or its immediate neighbors. This constraint reduced the detection efficiency by about 25%, but was very efficient in removing background. As an example we show in Fig. 4 data from a $dp \to dn\pi^+$ production run and the distribution of the reconstructed missing mass of the neutron. Application of the delayed hit criterion was accompanied by detailed Monte Carlo simulations and an experimental verification of the π^+ decays with the correct half life of the μ^+ decay.

III. REACTION MODELS AND MONTE CARLO SIMULATIONS

A. Quasifree pion production $dp \to Nd\pi$

In a truly quasifree dp reaction, two of the nucleons interact with the third one acting as a spectator. This is schematically shown in Fig. 5(a). In the case of the $dp \to dp\pi^0$ reaction there are three possible NN processes that may contribute at the π^0 production vertex (i) $pn \to d\pi^0$, (ii) $pp \to pp\pi^0$, and (iii) $pn \to pn\pi^0$. It is argued in Ref. [8] that (i) dominates, because near threshold the cross section for (ii) is much smaller and because (iii) favors the population of the four body final state $ppn\pi^0$. Similarly, the quasifree reaction $dp \to nd\pi^+$ should be based on a $pp \to d\pi^+$ reaction.

The diagram Fig. 5(a) has been evaluated [8] by relating the differential $pd \to pd\pi^0$ cross section to the elementary

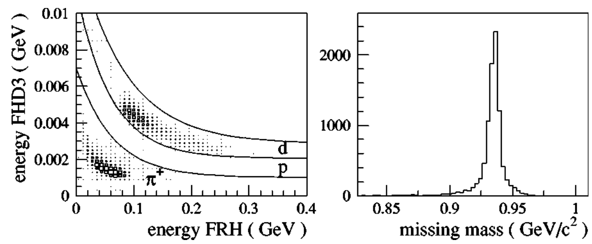

FIG. 4. E vs ΔE plots and missing mass distribution for $dp \to dn\pi^+$ events at $T_d = 559$ MeV.

process $pn \to d\pi^0$. We adopt this formalism for the two isospin related reactions studied in this paper in the generalized notation $dp \to N_s d\pi$. With the target proton being at rest it is obvious, that the pion production below the $2N$ threshold of the elementary process can only comply with momentum conservation through the momentum $\vec{\kappa}$ of the participating nucleon N in the projectile deuteron. The spectator nucleon N_s has consequently a momentum $\vec{p}_s = -\vec{\kappa}$. This gives rise to the probability density $|\Phi_d(\kappa)|^2$ of the nucleon momentum κ in the target deuteron to appear in the invariant matrix element of the spectator model:

$$|M|^2 = \frac{2E'_p E'_B E'_s}{E^*_N E^*_p} |\Phi_d(\kappa)|^2 |M_{pN \to d\pi}|^2. \tag{1}$$

Here, the first factor is a phase space factor which contains total energies of the target proton (p), the beam deuteron (B), and the spectator (s) in that $dp \to N_s d\pi$ reference frame where the final $d\pi$ subsystem is at rest (denoted by a prime), and total energies of the participating nucleons p, N in the center-of-mass system of the $pN \to d\pi$ reaction (denoted with an asterisk).

The invariant matrix element of the elementary $pN \to d\pi$ process is not derived from a microscopic model, but expressed using the experimental cross section $d\sigma_{pN\to d\pi}/d\Omega_{q*}(\cos\Theta^*_\pi)$ evaluated at $\eta^* = q^*/m_\pi c$:

$$|M_{pN\to d\pi}|^2 = 16(2\pi)^2 s_2 \frac{p^*_p}{q^*} \frac{d\sigma_{pN\to d\pi}}{d\Omega_{q*}}. \tag{2}$$

In Eq. (2) s_2 denotes the invariant mass squared of the $pN \to d\pi$ system, and p^*_p and q^* are the proton and pion momenta, respectively. $|\Phi(\kappa)|^2$ has been calculated from the Bonn potential [24] as incoherent sum of the S- and the D-state probability density. Insertion of Eq. (2) in Eq. (1) then provides *absolute* cross sections based on the experimental cross sections for $pn \to d\pi^0$ [25] and $\pi^+ d \to pp$ [26], the latter being related by isospin invariance and detailed balance to the former. A Legendre polynomial expansion has been fitted to the data for $\eta \leq 1$,

$$\frac{d\sigma_{pn\to d\pi^0}}{d\Omega_{q*}}(\cos\Theta^*_\pi) = \frac{\sigma_{pn\to d\pi^0}(\eta)}{4\pi} + a_2(\eta) P_2(\cos\Theta^*_\pi) \tag{3}$$

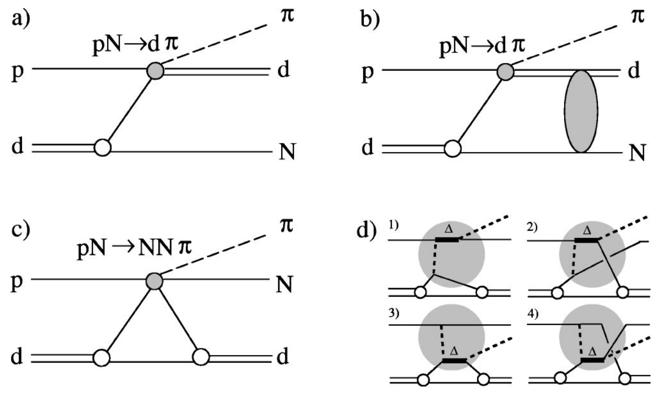

FIG. 5. Diagrams for $pd \to Nd\pi$ near threshold: QF pion production via $pN \to d\pi$ without (a) and with (b) pd-FSI; QF process $pN \to pN\pi^0$ without (c) and with (d) Δ resonance excitation. Open circles denote the deuteron wave function and filled ones reaction amplitudes.

yielding $a_2(\eta)=(47.2\ \ \mu\mathrm{b})\eta^3$. The angle integrated cross section is given by [25]

$$\sigma_{pn\to d\pi^0}(\eta)=\frac{1}{2}(c_1\eta+c_3\eta^3) \tag{4}$$

with $c_1=184\ \ \mu$b and $c_3=781\ \ \mu$b. The η^3 dependence reflects the pion p wave contribution. For the isospin related elementary reaction $pp\to d\pi^+$ the cross sections in Eqs. (3) and (4) are multiplied by a factor of 2.

B. Partial wave expansion

The spin degrees of freedom of the final three-body state ψ_f are described with the quantum numbers L, S, j, l, and J as follows: L and S denote the total orbital angular momentum and spin of the Nd subsystem coupled to $\vec{j}=\vec{L}+\vec{S}$. With the angular momentum l of the pion with respect to the center-of-mass of the Nd system, the total angular momentum J is obtained, viz. $\vec{J}=\vec{j}+\vec{l}$. The eigenstates contributing to the $pd\to Nd\pi$ transition can be grouped into partial waves Ll [27]. For an expansion into partial waves, the three-body wave function $\psi_f(\vec{p}_N,\vec{p}_d,\vec{p}_\pi)$ is factorized as $\psi_{Nd}(\vec{p}_{Nd})\cdot\psi_\pi(\vec{q})$, where $\vec{p}_{Nd}$ denotes the momentum of the relative motion in the Nd system, and $\vec{q}$ the momentum of the pion with respect to this subsystem. The relatively high momentum transfer of ≈ 400 MeV/c makes the interaction of short range, and one can employ a zero-range approximation [28] to calculate the transition matrix element $|M_{Ll}|^2$ for the partial waves

$$|M_{Ll}|^2 \propto |\vec{p}_{Nd}|^{2L}|\vec{q}|^{2l}. \tag{5}$$

In addition, $|M_{Ll}|^2$ depends on the angle Θ_π of the pion in the center of mass and the direction of the outgoing nucleon in the Nd rest system Θ_N both with respect to the direction of the incoming proton. The Ss wave has no angular dependence; p (P) waves give rise to two components $|M_{Lp}|^2 \propto q^2$ and $\propto q^2\cos^2\Theta_\pi$ ($|M_{Pl}|^2 \propto p_{Nd}^2$ and $\propto p_{Nd}^2\cos^2\Theta_N$) [28]. Furthermore we assume that the expansion can be limited to the lowest partial waves close to threshold ($\eta \leqslant 0.86$), viz.

$$|M|^2=|M_{Ss}|^2+|M_{Sp}|^2+|M_{Ps}|^2+|M_{Pp}|^2+|M_{Pd}|^2. \tag{6}$$

The sp and SP interference give rise to additional terms linear in $\cos\Theta$ whereas the d waves introduce $\cos^n\Theta_\pi$ dependencies with $n\geqslant 3$, too.

An attempt to determine the partial wave amplitudes from a fit of Eq. (6) to experimental data as it was done, e.g., in Ref. [29] for $pp\to pp\pi^0$ is of interest. One can confront the contributions of different spin and angular momentum eigenstates, e.g., the onset of pionic p and d waves above threshold, to reaction or potential models; and their orthogonality allows for an extrapolation into the regions of phase space not covered by the detector. This way one can determine detection efficiencies and total cross sections.

For the $dp\to Nd\pi$ case, however, the number of eigenstates contributing is too high for a rigorous separation of the individual amplitudes or the different transition classes Ll as, e.g., done for $pp\to pn\pi^+$ by Pleydon *et al.* [30]. In addition the partial wave approach neglects the extension and structure of the deuteron. We therefore restrict this expansion in two aspects: We fit only those fractions of the experimental distributions that are at variance with the QF approach of Eq. (1), and we consider only the dominant terms describing momentum and angle dependence, neglecting all interference effects. Details are given in Sec. IV C.

C. Final state interaction

In $dp\to dN\pi$ there are three candidates for two-body final state interactions (FSIs): πd, πN, and Nd. The application of the Watson-Migdal treatment of FSI [16] requires the relative momentum k and the distance between the interacting particles to be small, and the FSI to be strong compared with the short range primary interaction, here the pion production. Under these assumptions the transition probability including FSIs is proportional to the elastic scattering cross section, viz. $|M_{\mathrm{FSI}}(k)|^2 \propto \sigma_{\mathrm{FSI}}(k)$. Since both πd and πN scattering are weak, Nd-FSI will dominate.

$\sigma_{\mathrm{FSI}}(k)$ is calculated in S-wave approximation for Nd scattering as an incoherent, weighted sum of the channel-spin doublet (D) and quartet (Q) cross sections

$$\sigma_{\mathrm{FSI}}(k)=\frac{4\pi}{C_0(k)^2k^2}\left[\frac{1}{3}\sin^2\delta_s^D+\frac{2}{3}\sin^2\delta_s^Q\right], \tag{7}$$

where δ_s^D and δ_s^Q are the respective phase shifts and $C_0(k)$ is the Coulomb penetration factor (that is unity for nd-FSI). The numerical values for the phase shifts were obtained from [31] which uses an effective-range expansion fitted to pd scattering data for momenta $k\leqslant 180$ MeV/c, and similarly in [32] from nd scattering data for $k\leqslant 140$ MeV/c. As $k\to 0$, the pd cross section and thus the weighting factor $\sigma_{\mathrm{FSI}}(k)$ vanishes due to the Coulomb barrier, whereas the nd cross section is not influenced and σ_{FSI} reaches its maximum. Following [8] the values σ_{FSI} of Eq. (7) can be applied in the QF approach [Fig. 5(b)] as (normalized) weighting factors to the matrix elements (1). This way the modified energy dependence due to FSI is taken care of, causing the cross sections to be renormalized. This weighting may also be applied to the matrix element $|M_{Ll}|^2$ of any partial wave, in particular to the constant matrix element $|M_{Ss}|^2$, to modify the pure phase space distribution accordingly. The impact of this FSI will be examined for both models in Sec. IV.

D. Monte Carlo simulation and detector efficiency

The experiment and the analysis were accompanied by a comprehensive Monte Carlo (MC) simulation, based on GEANT [33], including details of the detector geometry, energy and angular straggling, secondary hadronic interactions in the detector material and decays of short lived particles. Events could be generated either evenly distributed or with a weighting proportional to the squared transition matrix elements $|M|^2$ according to Eqs. (1), (6), and (7). The resulting events were then tracked through a thoroughly tested MC model of the whole experiment including the actual trigger conditions, electronic settings and vertex distribution [2,34]. The MC events were analyzed with the same method as for experimental events for direct comparison with the experimental results.

Judged on the extent of agreement between the experimental distributions and reconstructed, MC generated events depending on the reaction model used, a best description of the reaction mechanism is approached. It leads to (i) a decomposition of the reaction mechanism into incoherent contributions of the reaction models included in the event generation; (ii) the total reaction cross sections, and (iii) the detector efficiency, the latter two being dependent on the event generator chosen. The technical details are given in Sec. IV C and IV D.

The main sources of detector inefficiency were the limited angular acceptance of deuterons and protons ($\Theta \geqslant 4^0$) due to the beam pipe and of the γ from π^0 decay in trigger mode TII. This reduces the acceptance typically by factors of 3 and 10, respectively. As an example we present simulations for the pure QF process at a projectile energy slightly above the $2N \rightarrow 2N\pi$ threshold in Fig. 6 together with the distributions of accepted $dp\pi^0$ events. They amount to $\approx 33\%$ for trigger TI and 10% for TII, with little variation over the accessible phase space. A further reduction by $\approx 25\%$ occurs with the π^+ identification for the $dp \rightarrow dn\pi^+$ channel.

IV. OFFLINE ANALYSIS AND DISCUSSION OF RESULTS

A. Event separation

Separation of $dp \rightarrow dp\pi^0$ requires both p and d being identified in the forward detector. Additional cuts on energy and angle were applied along the kinematical limits in accordance with the finite experimental resolution. Due to the short range of the dp pair for the two projectile energies closest to threshold, the last layers of the FRH could safely be used to veto punch-through protons from break up or bremsstrahlungs reactions. Trigger TII required, in addition, one photon with an energy deposition of at least 10 MeV in the CD. As a result, a clean π^0 signal is seen in the missing mass vs missing energy distribution reconstructed from the dp pair as shown in Fig. 7, and a clear separation from the bremsstrahlungs events $dp \rightarrow dp\gamma$ is obtained [35]. Therefore our event separation was based on the trigger TII for all projectile energies but the lowest, 436 MeV, where the low cross section requires the higher efficiency of TI. The numbers of identified events are listed in Table I. The $dp \rightarrow dn\pi^+$ events could clearly be identified with the two forward going charged particles and the reconstructed neutron mass. The numbers of events found at the three projectile energies 492, 515, and 559 MeV are given in Table I. At the lower energies the majority of deuterons escape through the beampipe leaving too few detected events to be analyzed.

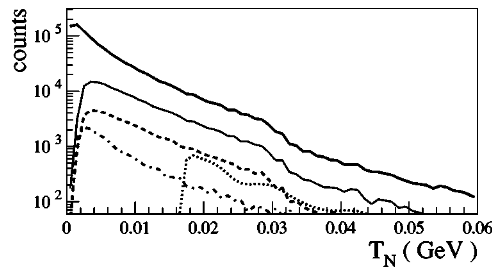

FIG. 6. MC generated response of the PROMICE/WASA experiment to the spectator energy spectrum in the primary deuteron rest frame for $T_d = 559$ MeV (thick solid line) of $dp \rightarrow dp\pi^0$ events ($\eta = 0.86$) with trigger options TI (thin solid line) and TII (dashed), and for $\rightarrow dn\pi^+$ (dash-dotted, $\eta = 0.78$). Also shown is the corresponding response (dotted) for the pd study at IUCF [17] for $\eta = 0.89$.

B. Observables in $dp \rightarrow dp\pi^0$

The direct experimental observables are the laboratory angles Θ_p, Θ_d and energies T_p, T_d of the dp pairs , as well as their opening angles $\angle_{dp}$ and coplanarities $\Delta\Phi_{dp} = \Phi_d - \Phi_p$. These are shown in Fig. 8 for the projectile energy 559 MeV. The deuteron energy that allows an elementary $pn \rightarrow d\pi^0$ process with no internal motion involved ($\kappa \approx 0$) is about 10 MeV lower, such that the kinematical hindrance of the spectator mechanism is only 0.5 as compared to 10^{-3} near the $3N$ threshold.

The spectator protons are expected to have their energy distributions peaking at half the projectile energy and at a low angle. In contrast, the experimental data extend to smaller energies and larger angles, indicating that a substantial momentum transfer to the deuterons is involved. For such events the deuteron energy distribution shows an excess at high energies. The excess of events with large opening angles $\angle_{dp}$ also has to be attributed to transverse momenta transferred to the proton, because the deuteron angles are kinematically limited to $\Theta_d < 15^0$. These qualitative features were also confirmed in an event selection that allowed the proton to escape down the beam pipe. It required only a deuteron in the forward detector in coincidence with a π^0 identified by its 2γ decay in the central detector.

The importance of pd-FSI was studied with the Watson-Migdal approach. At the $2N$ threshold, the $|\Phi(\kappa=0)|^2$

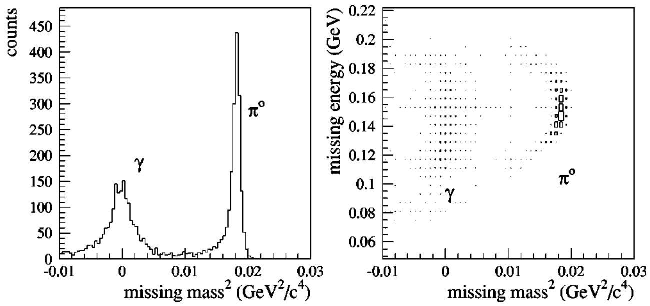

FIG. 7. Missing mass distributions at $T_d = 455$ MeV to an identified dp pair in the FD, accompanied by one γ in the CD.

weighting in the quasifree model favors relative momenta $k \approx 250$ MeV/c, where FSI is small and not much k dependent. The attractive FSI is expected to decelerate the faster proton and accelerate the slower deuteron. Figure 9 compares proton and deuteron distributions as predicted from quasifree interaction with and without FSI. There is no visible influence on the angular distribution of the spectator proton or the reaction deuteron; the energy distributions shift as expected, however, to an extent that is too small to account for the observed (see Fig. 8) difference between experiment and quasifree prediction. There must be another reaction mechanism beyond that of the quasifree model, be it with or without FSI.

C. $dp \rightarrow dn\pi^+$ and phase space coverage

The observables of the detected $d\pi^+$ pairs correspond to those of the dp pairs for $dp \rightarrow dp\pi^0$, i.e., $\Theta_d, \Theta_{\pi^+}, T_d, T_{\pi^+}$, the opening angle $\angle_{d\pi^+}$, and the coplanarity $\Delta\Phi_{d\pi^+}$. The distributions for T_d and Θ_d in Fig. 10 for the projectile energies 559 MeV ($\eta = 0.78$) and 515 MeV ($\eta = 0.62$) show similar deviations from the QF model as were already seen for $dp \rightarrow dp\pi^0$ in Fig. 8. The π^+ with its small momentum and narrow energy distribution, however, cannot contribute much to this discrepancy. This indicates that the supposed spectator neutron must have acted as participant. Indeed, the distributions for T_n and Θ_n reconstructed from the direct observables show similarity to those for the outgoing proton in $dp \rightarrow dp\pi^0$.

It is important to confirm that the sensitivity of the experiment to different reaction models is not severely hampered by the acceptance of the PROMICE/WASA detector. This has been tested by simulating the acceptance for two extreme cases of initial phase space population, namely, the uniform Ss wave coverage and the spectator model distribution proportional to the squared matrix element of Eq. (1). The results for both reaction channels $dp\pi^0$ and $dn\pi^+$ are shown in Fig. 11 as Dalitz plots.

The dynamic variables used for $dp \rightarrow dN\pi$ are dimensionless combinations of the squared invariant masses s_{ab} in the subsystem ab with $x \propto s_{N\pi} - s_{d\pi}$ and $y \propto s_{Nd}$ and a normalization that removes the dependence of the Dalitz plot contour on the total invariant mass. The first row of Fig. 11 demonstrates that the two reaction channels are complementary with respect to the accessible phase space, which can be

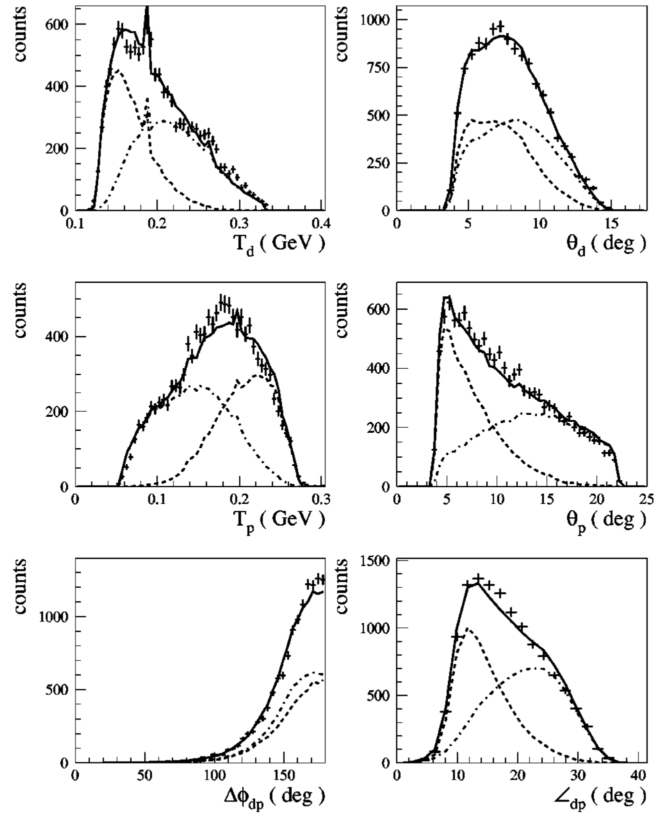

FIG. 8. Experimental angular and energy distributions of the $dp \rightarrow dp\pi^0$ observables (crosses) at $T_d = 559$ MeV in comparison to a best fit (solid line) composed of a quasifree (QF, dashed) and a partial wave (SF, dash-dotted) contribution.

traced back to the two charged particles requested in the FD for triggering. The quasifree reaction model (second row) generates a population with two maxima corresponding to a pion going backward ① or forward ② in the $Np \rightarrow d\pi$ center-of-mass frame. The detection of the forward going π^0

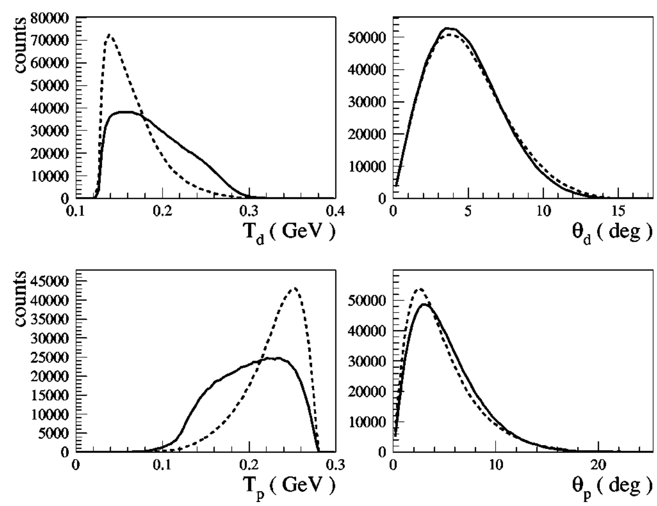

FIG. 9. Energy and angular distributions of deuterons and protons from $dp \rightarrow dp\pi^0$ events generated for a pure QF mechanism and $T_d = 559$ MeV without (dashed line) and with (solid line) dp-FSI. The detector acceptance is not included.

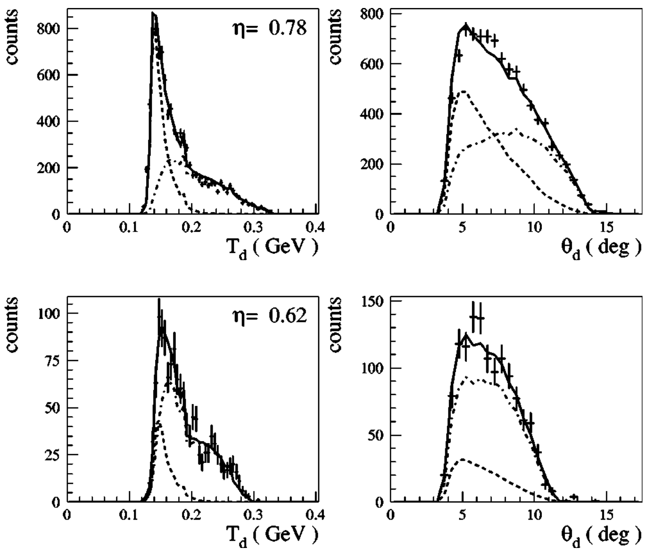

FIG. 10. Comparison of the experimental deuteron observables (crosses) for $dp \to dn\pi^+$ at $T_d = 559$ MeV (top) and 515 MeV (bottom) to the best fit (solid line) with QF (dashed) and SF (dash-dotted) contributions.

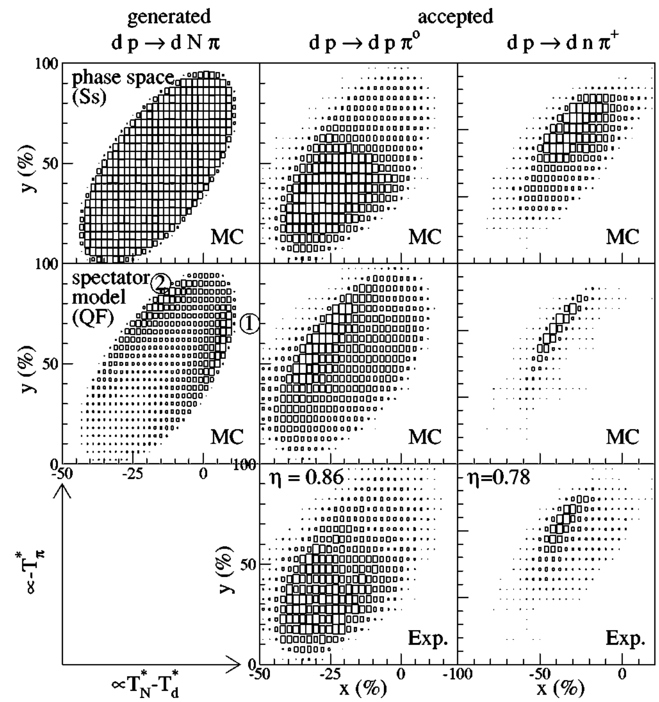

FIG. 11. Dalitz plots for $dp \to dN\pi$ at $T_d = 559$ MeV. The first column shows the MC generated distributions for a constant matrix element (*Ss*, first row) and for the QF mechanism (second row). The accepted events are for $dp \to dp\pi^0$ ($dp \to dn\pi^+$) in the center (right) column; the corresponding experimental results are in the bottom row. (See text for details.)

or π^+ is favored by the detector geometry; the partial suppression of the backward going pion makes the detector less sensitive to terms in Eq. (6) linear in $\cos\Theta_\pi$. The two reaction channels complement each other in such a way, that a sensitivity to both generated phase space populations should result. Indeed, the experimental data in the bottom row for both reactions show copious events in excess of the QF model.

In order to quantify the extent to which the quasifree model can reproduce the data, a fitting procedure to the direct observables has been applied. The idea is to compare the distributions of all observables in the laboratory frame with distributions resulting from the matrix elements of Eqs. (1) and (6), and to fix their relative contributions in a simultaneous best fit to *all* data of one reaction channel at a given projectile energy.

D. Incoherent decomposition of experimental distributions

Let $x(i,j)$ be the number of events in bin j of the distribution of the ith out of I experimental observables ($I \leqslant 6$) and $m_k(i,j)$ the corresponding number for reconstructed MC events from a simulation of N_0 events generated with the reaction model k. The experimental result shall then be best fitted with the incoherent sum of K reaction mechanisms, viz.

$$f(i,j) = \sum_{k=1}^{K} c_k m_k(i,j) \tag{8}$$

by varying the parameters $c_k \geqslant 0$ for a minimum of

$$\chi^2(c_1, \ldots, c_N) = \sum_{i=1}^{I} \frac{1}{J(i)} \sum_{j=1}^{J(i)} \frac{[x(i,j) - f(i,j)]^2}{x(i,j)}. \tag{9}$$

Here, $J(i)$ is the number of bins with event numbers $x(i,j) > 0$ for the observable i. From the total number $N_{\mathrm{gen}} = N_0 \Sigma_{k=1}^{K} c_k$ of generated events, a fraction $dN_{\mathrm{gen}}(\tau_{ps})$ will populate the phase space bin $[\tau_{ps}, \tau_{ps} + d\tau_{ps}]$. With $dN_{\mathrm{rec}}(\tau_{ps})$ being the fraction of reconstructed events, the resulting detection efficiency is given by

$$\epsilon_{\mathrm{MC}}(\tau_{ps}) = \frac{dN_{\mathrm{rec}}(\tau_{ps})}{dN_{\mathrm{gen}}(\tau_{ps})}. \tag{10}$$

We assume now that the best fit gives a good description of the experimental results for all observables and phase space bins accessible, viz.

$$dN_{\mathrm{exp}}(\tau_{ps}) \approx dN_{\mathrm{rec}}(\tau_{ps}), \tag{11}$$

and also a realistic description of the PROMICE/WASA detector performance: $\epsilon_{\mathrm{PW}}(\tau_{ps}) \approx \epsilon_{\mathrm{MC}}(\tau_{ps})$. This fit procedure has been applied at each projectile energy to all six observables of the reaction $dp \to dp\pi^0$ and to five observables from $dp \to dn\pi^+$; in the latter case T_{π^+} was excluded, because it is prone to larger systematic errors.

The following partial waves were included in the fit in addition to the spectator model: Ss, Ps (isotropic and anisotropic in Θ_N), Sp, Pp (isotropic and anisotropic in Θ_N), Pd (isotropic and anisotropic in Θ_N). The terms anisotropic in Θ_π (Sp, Pp, Pd) have been omitted as well as the s-p and S-P interference terms. This omission was preceded by several tests including all or some of these terms; they showed that the fit quality was not sensitive to them and that their coefficients c_k indicated only small contributions. In particular the fraction attributed to the QF model did not depend on the terms omitted. The sum of partial wave terms is used to

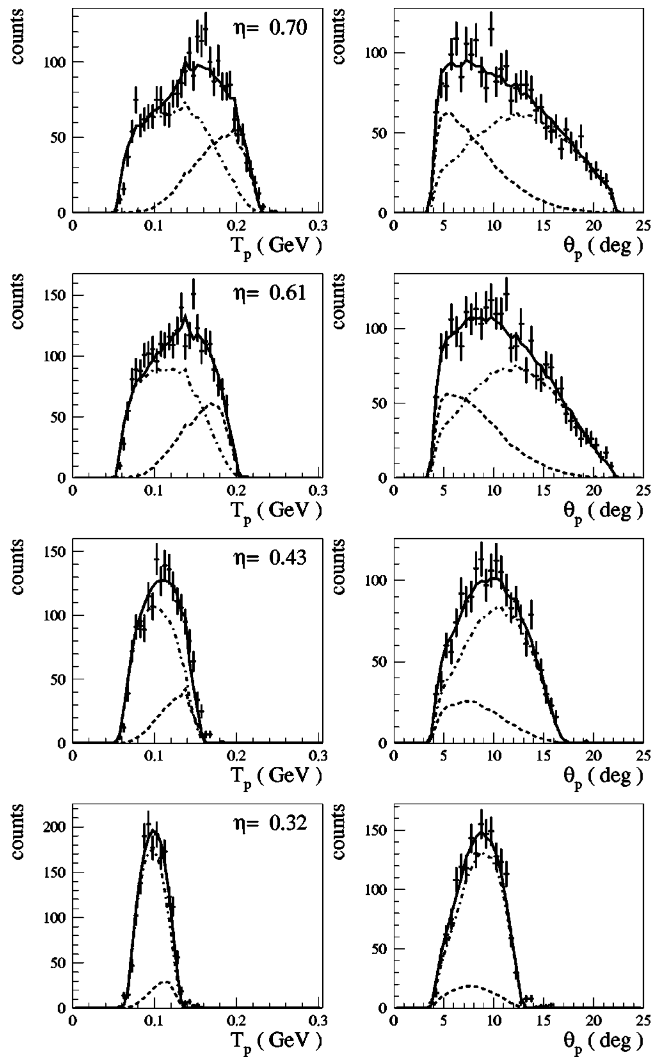

FIG. 12. Comparison of the experimental proton observables (crosses) for $dp \rightarrow dp\pi^0$ at the indicated projectile energies (η values) to the best fit (solid line) with QF (dashed) and SF (dash-dotted) contribution.

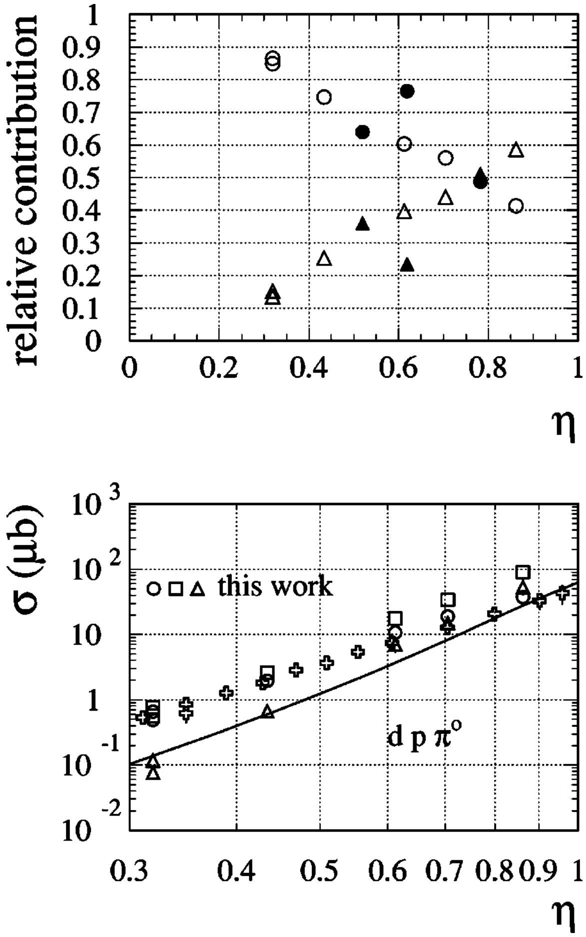

FIG. 13. Top: Relative contributions of the QF (triangles) and SF (circles) production mechanism to the distributions of observables in $dp \rightarrow dp\pi^0$ (open symbols) and $dp \rightarrow dn\pi^+$ (closed symbols). Bottom: Comparison of the $dp \rightarrow dp\pi^0$ excitation function $\sigma(\eta)$ of this work (open squares) and its decomposition into QF (open triangles) and SF contribution (open circles) with the result from Ref. [17] (open crosses). The line gives the prediction of the spectator model [8] without pd-FSI.

describe the yield incompatible with the spectator model and is hereafter referred to as selected fit (SF).

Figures 8 and 10 (top) show for the projectile energies close to the $2N$ pion production threshold, that an excellent fit can be obtained simultaneously for all observables, with the QF part accounting for about half the observed yield. The salient features of these best fits are also visible at lower projectile energies; a selection of observables with sensitivity to the two reaction components for $0.32 \leqslant \eta \leqslant 0.71$ is shown in Fig. 12. Upon approach of the $3N$ threshold for pion production, the fraction of events attributed to a QF mechanism decreases. At the same time, however, the predicted shapes of the two reaction components approach each other while the distributions get altogether narrower and the event statistics lowers, because the particles tend to escape through the hole of the beam pipe. All this makes the fit results less accurate.

Lo *et al.* [14] have studied differential cross sections $d^3\sigma(p_d, \Theta_d, \Theta_\pi)$ of the $pd \rightarrow nd\pi^+$ reaction far above threshold ($T_p = 800$ MeV, $\eta = 3.1$) in a kinematically complete experiment with a two arm spectrometer. They find that QF is the dominant mechanism in that region of phase space where the target neutron recoils with zero momentum, i.e., in $pp \rightarrow d\pi^+$ geometry. In regions with higher (100 MeV/c) momentum transfer, however, the spectator model underestimates the experiment suggesting that other mechanisms contribute noticeably. Hogstrom *et al.* [13] concluded from a similar experiment at $T_p = 585$ MeV ($\eta = 2.3$) in regions with neutron recoil momenta $\geqslant 400$ MeV/c that several mechanisms involving all three nucleons [as, e.g., in Figs. 5(c), 5(d)] contribute and that the one nucleon exchange process of Fig. 5(a) is heavily suppressed. From the analysis of these results Duck *et al.* [36] conclude that double scattering amplitudes with a Δ produced at the first collision determine the gross features of the differential cross sections.

E. Total cross sections

With reference to the fit results of Eq. (9) we can extrapolate the experimental information on the event generator level into phase space regions not covered by the detector acceptance. The differential cross section for population of the phase space bin is obtained from Eqs. (10), (11) as

$$d\sigma(\tau_{ps})=\frac{1}{L_{\rm int}}\frac{dN_{\rm exp}(\tau_{ps})}{\epsilon_{\rm PW}(\tau_{ps})}=\frac{1}{L_{\rm int}}dN_{\rm gen}(\tau_{ps}), \qquad (12)$$

where $L_{\rm int}$ denotes the integrated luminosity. Integration of Eq. (12) over finite regions of the phase space yields the corresponding cross sections and, in particular, the total cross section of a reaction is obtained as

$$\sigma_{\rm tot}=\frac{1}{L_{\rm int}}N_{\rm gen}=\frac{N_0}{L_{\rm int}}\sum_{k=1}^{K}c_k=\sum_{k=1}^{K}\sigma_{{\rm tot},k} \qquad (13)$$

such that the best fit coefficients c_k eventually provide the decomposition of $\sigma_{\rm tot}$ into the contributions $\sigma_{{\rm tot},k}$ of the reaction models given in Fig. 13. For $dp\rightarrow dp\pi^0$ the fraction attributed to the quasifree process increases almost linearly from 13% for both measurements at $\eta=0.32$ to 59% at $\eta=0.86$. These numbers depend on the event generator applied for extrapolation into the phase space not seen by the detector and may therefore vary with the event selection criteria. Alternative criteria, e.g., the requirement of one identified deuteron in the FD in conjunction with two γ's from the π^0 decay in the CD and a missing mass identification of the supposed spectator proton, have been applied. The spectral and angular distributions of these deuterons always required similar SF contributions relative to the QF component.

The fractions deduced from $dp\rightarrow dn\pi^+$ scatter around this trend. For $\eta=0.62$, a deviation by 15% from the $dp\rightarrow dp\pi^0$ data is observed, which is considered an outcome of the limited acceptance and statistics for the two lower projectile energies (see Table I) rather than a systematic effect.

The total cross sections $\sigma_{\rm tot}$ obtained with Eq. (13) are listed in Table I together with the error estimates. The numbers $N_{dN\pi}$ of events in Table I correspond to statistical errors $\delta_N\leqslant 3\%$. The detection of charged particles discussed in Sec. II E is associated with systematic uncertainties. Proton identification capabilities of the PROMICE/WASA setup have been studied in previous experiments as well as with MC simulations and are estimated to be very accurate ($\delta_p\leqslant 1\%$); the deuteron detection is influenced by secondary reaction losses, in particular breakup processes ($\delta_d\leqslant 15\%$). The π^+ identification with the delayed pulse technique has an inaccuracy $\delta_{\pi^+}<15\%$. The uncertainties δ_L of the luminosity monitor were already given in Sec. II C.

The errors $\delta_{\rm accept}$ resulting from the extrapolation of the phase space population into regions not covered by the detector acceptance are estimated from several best fit attempts under varying selection criteria for $dp\rightarrow dp\pi^0$ to be $<10\%$. For $dp\rightarrow dn\pi^+$ the acceptance is, mostly due to the restricted angular coverage for π^+ detection, too small to give a reliable error estimate. Charge symmetry requires a factor of 2 for the cross section ratio $\sigma(dp\rightarrow dn\pi^+)/\sigma(dp\rightarrow dp\pi^0)$. At least this qualitative relation is fulfilled and excludes excessive values of $\delta_{\rm accept}$ for the π^+ production.

We now turn to the discussion of the excitation functions for $dp\rightarrow dp\pi^0$ that are compared in Fig. 13 (bottom) with the results from Ref. [17]. For $\eta\leqslant 0.45$ both excitation functions are in good agreement although the two experimental setups cover different regions of the phase space: The pd experiment [15] is essentially blind to the QF interaction, because a spectator proton would come from the target deuteron at rest and could be detected only with a minimum (see Fig. 6) of 17 MeV kinetic energy resulting from the internal motion. Our dp experiment in contrast has a comfortable acceptance for the spectator protons, since these move with about half the projectile deuteron energy and need only a small transverse momentum component for being detectable.

The observed agreement therefore leads to the conclusion that the QF fraction of the total $pd\rightarrow pd\pi^0$ cross section can only be small; the reaction products must rather generate a smooth distribution in phase space that allows a good extrapolation into the region not accessed. This applies in particular to distributions resulting from transition matrix elements $|M_{Ss}|^2,|M_{Ps}|^2$, and $|M_{Sp}|^2$ that dominate the SF representation [17,35]. It should be stressed that the IUCF experiment [15] was designed for this momentum range ($\eta<0.4$).

Indeed Fäldt and Wilkin [37] have found that close to threshold ($\eta\leqslant 0.35$) the $pd\rightarrow pd\pi^0$ excitation function can be related to that of the corresponding binary reaction $pd\rightarrow {}^3{\rm He}\pi^0$ [38,39]. Their calculation assumes S wave dominance in the final dp system and needs no assumption on the

TABLE I. Experimental conditions, total cross sections, and error estimates for $dp\rightarrow dp\pi^0$ ($dp\rightarrow dn\pi^+$)

E_d MeV	$L_{\rm int}$ 10^{34} cm^{-2}	$\eta_{dp\pi^0}$ ($\eta_{dn\pi^+}$)	Trigger	$N_{dp\pi^0}$ ($N_{dn\pi^+}$)	$\sigma_{\rm tot}$ μb	$\delta\sigma_N$ %	$\delta\sigma_d$ %	$\delta\sigma_{p,\pi^+}$ %	$\delta\sigma_L$ %	$\delta\sigma_{\rm accept}$ %
436.7	2.57	0.32	dp	1949	0.57 ± 0.12	2	15	1	10	10
436.7	1.74	0.32	dp	1747	0.77 ± 0.19	2	15	1	17	10
454.7	2.14	0.43	$dp\gamma$	1820	2.6 ± 0.5	2	15	1	10	10
491.8	1.59	(0.52)	$d\pi^+$	(971)	20 ± 6	3	15	15	17	–
491.8	1.59	0.61	$dp\gamma$	2643	18 ± 4	2	15	1	17	10
514.8	0.71	(0.62)	$d\pi^+$	(1274)	47 ± 12	3	15	15	10	–
514.8	0.71	0.71	$dp\gamma$	2416	34 ± 7	2	15	1	10	10
559.0	1.72	(0.78)	$d\pi^+$	(9206)	144 ± 42	1	15	15	17	–
559.0	1.72	0.86	$dp\gamma$	12 480	90 ± 22	1	15	1	17	10

π^0 wave. A reasonable description of the excitation function is obtained which indicates a preference for the dp spin-doublet over the spin-quartet state. This is at variance with a statistical population as in the QF mechanism, see Eq. (7).

For $\eta > 0.45$ the QF contribution to σ_{tot} becomes increasingly important. Here, the two excitation functions $\sigma_{\mathrm{tot}}(\eta)$ disagree by a factor up to 3. Based upon Eq. (13) we can decompose our result σ_{tot} into the two excitation functions $\sigma_{\mathrm{QF}}(\eta)$ for the QF process and $\sigma_{\mathrm{SF}}(\eta)$ for the SF component. The agreement between σ_{SF} and the result for σ_{tot} of Ref. [17] in Fig. 13(b) for the whole range $\eta \leqslant 1$ is remarkable; indeed it seems that the disagreement in σ_{tot} is essentially due to the missing QF component in the data of Refs. [15,17].

Our excitation function $\sigma_{\mathrm{QF}}(\eta)$ agrees in η dependence as well as in absolute units within a factor of 2 with the calculation [8] of the QF process using the matrix element of Eq. (1). The (relative) excitation function calculated for the QF mechanism with pd-FSI enhances the excitation function only for lower η such that the agreement with our experimental data $\sigma_{\mathrm{QF}}(\eta)$ is lost. And what is the impact of a pd-FSI on the decomposition of the total cross section at one projectile energy? As already shown in Fig. 9 for the Watson-Migdal approach it has moderate influence on the spectral and none on the angular distributions of the ejectiles. Inclusion of this FSI in the spectator model component applied in the fitting procedure led to fractions compatible with the trends in Fig. 13, however, with systematically higher χ^2. Based on our data, the pd-FSI seems therefore insufficient and inadequate to account for the deviations from the QF model calculations.

V. SUMMARY

The reactions $dp \rightarrow dp\pi^0$ and $dp \rightarrow dn\pi^+$ have been studied in a kinematically complete experiment at five deuteron projectile energies between the thresholds for the $dN \rightarrow dN\pi$ and a QF $NN \rightarrow NN\pi$ process. Spectroscopy of the forward going charged particles was performed with the PROMICE/WASA setup; the third neutral particle was either identified by its missing mass (n,π^0), or by the $\pi^0 \rightarrow \gamma\gamma$ decay. Concurrent measurement of the elastic dp scattering provided the reference data for absolute cross sections.

The detector efficiency was derived by extrapolating the reaction yield into phase space regions not covered by the detector acceptance. This calculation was based on an incoherent combination of the QF process [8] and a mechanism parametrized in a partial wave expansion (SF) best fitting the observed yields.

For $dp \rightarrow dp\pi^0$, the angular and spectral distributions of the supposed spectator proton to an elementary $np \rightarrow d\pi^0$ process are observed in phase space regions where it is kinematically favored by a zero recoil momentum. Close to threshold the necessary recoil momentum in the order of 200 MeV/c has to come from the momentum distribution in the projectile deuteron; this makes the QF mechanism a rare process. With increasing η the recoil momentum needed decreases and can be provided with higher probability from the Fermi motion enhancing the QF process.

Altogether, however, the outgoing protons clearly indicate a preference for momentum transfers higher than those expected from a QF process and point towards a mechanism involving all three nucleons. A Watson-Migdal type pd-FSI alone cannot account for this discrepancy, because it does not extend the range of transferred momenta, and it is not compatible with the weight that must be given to P wave contributions. If genuine $3N$ forces, e.g., of the Tucson-Melbourne type are excluded [6,21], double scattering amplitudes of the kind discussed in Ref. [36] may be promising candidates for a coherent description of all observables in terms of reaction models.

In order to give a more quantitative estimate of the QF contribution without knowing details of the competing $3N$ reaction mechanism, we applied a fitting procedure that encompasses all non-QF contributions in a partial wave expansion neglecting interference effects. The resulting decomposition is consistent for both $dN \rightarrow dN\pi$ channels of this paper; it yields a fractional QF component that increases almost linearly with η and reaches 50–60 % at the $NN \rightarrow NN\pi$ threshold. According to Refs. [13,14] the QF mechanism does not exhaust the observed differential cross sections even far above ($\eta \geqslant 2.3$) threshold.

The excitation functions $\sigma_{pd\pi^0}(\eta)$ and $\sigma_{nd\pi^+}(\eta)$ differ by a factor of roughly 2 as expected from charge independence. Agreement with the results $\sigma_{pd\pi^0}(\eta)$ from Ref. [15] is obtained if it is assumed that there the QF component was either too small (for $\eta \leqslant 0.45$) or too much outside the detector acceptance to provide a substantial contribution. Our excitation function $\sigma_{\mathrm{QF}}(\eta)$ of the $dp\pi^0$ channel is in good agreement both in shape and in absolute values with the QF model [8] and no pd-FSI is needed.

ACKNOWLEDGMENTS

We thank D. Reistad and the operating team of the Cooler Synchrotron CELSIUS for excellent beam and target support. One of us (W.S.) thanks the TSL for the hospitality during his sabbatical stay. This work was partly supported by the German BMBF, Contract No. 06HH582.

[1] W. R. Falk, Phys. Rev. C **50**, 1574 (1994).
[2] H. Calén *et al.*, Phys. Rev. Lett. **79**, 2642 (1997).
[3] M. Benjamintz *et al.*, Phys. Rev. C **58**, 964 (1998).
[4] F. Duncan *et al.*, Phys. Rev. Lett. **80**, 4390 (1998).
[5] W. Glöckle, H. Witała, D. Hüber, H. Kamada, and J. Golak, Phys. Rep. **274**, 107 (1996).
[6] H. O. Meyer, in *Proceedings of the XVth International Conference on Few Body Problems in Physics, Groningen, The Netherlands, 1997*, edited by J. C. S. Baclear, A. E. L. Dieperink, and R. A. Malfliet (Elsevier Science, Amsterdam,

1998), p. 122c.

[7] M. Przyborowski, M. Eggert, R. Engels, M. Menzel, L. Sydow, H. Paetz gen. Schieck, H. Witała, J. Golak, J. Kuroś, and W. Glöckle, Phys. Rev. C **60**, 064004 (1999).

[8] H. O. Meyer and J. A. Niskanen, Phys. Rev. C **47**, 2474 (1993).

[9] H. O. Meyer, Annu. Rev. Nucl. Part. Sci. **47**, 235 (1997).

[10] J. Niskanen, Phys. Lett. B **456**, 107 (1999).

[11] I. A. Babalola, A. G. Forson, and F. A. N. Osadebe, Nucl. Phys. **B78**, 561 (1974).

[12] K. R. Hogstrom, Ph.D. thesis, Rice University, Houston, 1977.

[13] K. R. Hogstrom *et al.*, Phys. Rev. C **17**, 259 (1978).

[14] J. W. Lo *et al.*, Phys. Rev. C **20**, 1479 (1979).

[15] H. Rohdjeß *et al.*, Phys. Rev. Lett. **70**, 2864 (1993).

[16] K. M. Watson, Phys. Rev. **88**, 1163 (1952); A. B. Migdal, Zh. Éksp. Teor. Fiz. **28**, 3 (1955) [Sov. Phys. JETP **1**, 2 (1955)].

[17] H. Rohdjeß, Ph.D. thesis, Universität Hamburg, Hamburg, 1994.

[18] C. Ekström, Nucl. Instrum. Methods Phys. Res. A **362**, 1 (1995).

[19] M. Dahmen *et al.*, Nucl. Instrum. Methods Phys. Res. A **348**, 97 (1994).

[20] H. Calén *et al.*, Nucl. Instrum. Methods Phys. Res. A **379**, 57 (1996).

[21] H. Rohdjeß *et al.*, Phys. Rev. C **57**, 2111 (1998).

[22] J. Zabierowski, Nucl. Instrum. Methods Phys. Res. A **383**, 577 (1994).

[23] R. Madey, F. M. Waterman, A. R. Baldwin, J. N. Knudson, J. D. Carlson, and J. Rapaport, Nucl. Instrum. Methods **151**, 445 (1978).

[24] R. Machleidt, K. Holinde, and C. Elster, Phys. Rep. **149**, 66 (1987).

[25] D. A. Hutcheon *et al.*, Nucl. Phys. **A535**, 618 (1991).

[26] B. G. Ritchie *et al.*, Phys. Rev. Lett. **66**, 568 (1991); Phys. Rev. C **24**, 552 (1981).

[27] R. Handler, Phys. Rev. **138**, 1230 (1965).

[28] K. M. Watson and K. A. Brueckner, Phys. Rev. **83**, 1 (1951).

[29] J. Złomańczuk *et al.*, Phys. Lett. B **436**, 251 (1998).

[30] R. G. Pleydon *et al.*, Phys. Rev. C **59**, 3208 (1999).

[31] J. Arvieux, Nucl. Phys. **A221**, 253 (1974).

[32] W. T. H. van Oers and J. D. Seagrave, Phys. Lett. **24B**, 562 (1967).

[33] CERN Program Library Long Writeup W5013.

[34] S. Häggström, Ph.D. thesis, Universtet Uppsala, Uppsala, 1997.

[35] J. Greiff, Ph.D. thesis, Universität Hamburg, Hamburg, 1999.

[36] I. Duck, K. R. Hogstrom, and G. S. Mutchler, Phys. Rev. C **18**, 887 (1978).

[37] G. Fäldt and C. Wilkin, Phys. Lett. B **382**, 209 (1996).

[38] M. A. Pickar, A. D. Bacher, H. O. Meyer, R. E. Pollock, and G. T. Emery, Phys. Rev. C **46**, 397 (1992).

[39] V. Nikulin *et al.*, Phys. Rev. C **54**, 1732 (1996).